Submitted to Physica Status Solidi

LBL-2761
Preprint c.2

THE NATURE AND HABIT PLANES OF DEFECTS IN P^+ ION-IMPLANTED SILICON

K. Seshan and J. Washburn

June, 1974

Prepared for the U. S. Atomic Energy Commission
under Contract W-7405-ENG-48

TWO-WEEK LOAN COPY

This is a Library Circulating Copy which may be borrowed for two weeks. For a personal retention copy, call Tech. Info. Division, Ext. 5545

LAWRENCE BERKELEY LABORATORY • UNIVERSITY OF CALIFORNIA • BERKELEY

25

LBL-2761 c.2

DISCLAIMER

This document was prepared as an account of work sponsored by the United States Government. While this document is believed to contain correct information, neither the United States Government nor any agency thereof, nor the Regents of the University of California, nor any of their employees, makes any warranty, express or implied, or assumes any legal responsibility for the accuracy, completeness, or usefulness of any information, apparatus, product, or process disclosed, or represents that its use would not infringe privately owned rights. Reference herein to any specific commercial product, process, or service by its trade name, trademark, manufacturer, or otherwise, does not necessarily constitute or imply its endorsement, recommendation, or favoring by the United States Government or any agency thereof, or the Regents of the University of California. The views and opinions of authors expressed herein do not necessarily state or reflect those of the United States Government or any agency thereof or the Regents of the University of California.

THE NATURE AND HABIT PLANES OF DEFECTS IN P^+ ION-IMPLANTED SILICON

K. Seshan and J. Washburn

Inorganic Materials Research Division, Lawrence Berkeley Laboratory and Department of Materials Science and Engineering, College of Engineering; University of California, Berkeley, California 94720

ABSTRACT

Several contradictions about the nature of defects formed on the annealing of P^+ ion-implantation damage in (111) silicon are resolved. It is confirmed that the defects are interstitial type. The analysis still does not determine the exact displacements associated with the defects. The 180° ambiguity in crystal orientation was resolved using the Kikuchi poles and the asymmetry of the dark field image of rod shaped defects.

The habit planes of the defects were determined using weak-beam techniques. The defects are shown to be hexagonal, faulted and lying on the four {111} planes with displacements of the type $\frac{a}{x}\langle 111\rangle$. This distribution of defects suggest that they are formed by the growth of interstital clusters on close packed planes.

1. Introduction

It is known that annealing of ion-implantation damage in silicon results in a debris of small defects. The characterization of these defects is difficult and has been plagued with contradictions because of their small size and complex image behavior.

Some workers have reported that the loops are perfect [1,2,3], and have Burgers vectors of the type $\frac{a}{2}\langle 110\rangle$, all inclined to the (111) foil plane [3]. It has been suggested [3] that most of the loops lie in the foil plane. These authors have proposed no explanation for the three missing loop families having $\frac{a}{2}\langle 110\rangle$ Burgers vectors that lie in the foil plane. Some of the loops in the foil plane also have been reported to be imperfect and vacancy type [4]. The habit planes of the inclined loops have not previously been determined. Recently a great majority of the defects have been shown to be interstitial type Frank (i.e. imperfect) loops.

Since earlier reports are contradictory and incomplete it is clear that a further investigation of defects in P^+ ion-implanted and annealed (111) silicon is needed. In this study, we have determined the type (interstitial or vacancy) of the defects, using conventional diffraction contrast analysis, as well as their habit planes using the weak-beam technique [6,6a].

2. Experimental

Samples of polished p-type (Boron doped) silicon implanted with 100 keV P^+ ions to a dose of 2×10^{14} i/cm^2 were supplied by the Fairchild Company R&D division. These were ultrasonically cut into discs of 2.3 mm and dished on the non-implanted side. They were then chemically thinned in a solution made up of two parts (3HNO:1HF) to one part (2.5 g I_2 in 1100 ml Acetic acid). The thinned samples were

examined in a Siemens 1A and a Philips 301 electron microscope.

3. Results

The conventions used for the projections are shown in Fig. 1. Given the diffraction pattern there is a 180° ambiguity in the orientation of the crystal. In Fig. 1b, it is shown that the ambiguity is resolved by noting the position of the [211] pole in the Kikuchi pattern. This information was found experimentally by tilting the crystal 18°. Figure 2 shows the stero pair obtained while tilting to determine the position of the [211] pole. Viewing Fig. 2a and Fig. 2b through a stereo-viewer shows that the linear rod like defect AC lies in the plane of the foil and that BD is inclined at a very steep angle to the foil surface. Marked below the micrographs are the corresponding tetrahedra. The change in the direction of the inclined rod BD can be directly correlated to the tilting of the crystal.

Figures 3a and 3b show how dark field images may also be used to eliminate the ambiguity by changing the sign of s, the deviation from exact Bragg orientation. The deviation s is defined as positive ($s>0$) when the reciprocal lattice point lies within the Ewald sphere (Fig. 1b). In Fig 3a ($s<0$) the top of the inclined rod (near the upper surface of the crystal) is in good contrast whereas in Fig. 3b ($s>0$) the bottom end of the rod D is seen in good oscillating contrast. Thus the sense of inclination of the rod BD is known [8] (B near the top of the crystal and D near the bottom of the crystal) and the tetrahedra correctly oriented are shown below the images in Figs. 3a and 3b.

4. Analysis of Loops on Inclined Planes

The correct tetrahedron as viewed above the crystal (taking into account the inversion involved in the Siemens Elmiskope I) is shown in Fig. 1b. This tetrahedron and the crystal shown below it are used for the formal analysis [7]. (The tetrahedron as seen in a positive print, emulsion down, is shown in Fig. 1a.) The correct crystallographic orientations can be found with the (111) stereogram shown in Fig. 1c. All micrographs used in the analysis are imaged with positive values of "s" the deviation parameter and printed emulsion down.

In the images used for analysis (Figs. 2a and 2b) the loop variant marked γ is assumed to lie inclined as the plane ABD and the loop marked β inclined as the plane ADC. For such small loops it is difficult to acertain the exact habit planes from bright field images, even by high angle (over 30°) tilting. The high normal and lateral strain fields around these small defects make the bright field images insensitive to the orientation of the core of the defect. To determine the habit planes of these defects we have used weak-beam microscopy.

5. Determination of Loop Habit Plane

In Section 4 it was assumed that the loops marked γ (Fig. 2a) lie on a plane inclined in the sense of the plane ADB and β in the sense of the plane ADC. It was, however, impossible to determine exactly the habit planes from the bright field images alone.

The habit planes have been determined using weak beam electron microscopy [6,6a]. In Figs. 4a and 4b the defects are imaged in weak beam at the [211] and at the [233] poles respectively. In Fig. 4a the variant marked β lying on the plane ADC appears edge-on while the loops

α and γ lie on inclined planes ADC and ADB. (The loop marked γ is cut by the foil surface.) Loops lying on the (111) plane, δ, appear hexagonal and support the view that all loops are equal sided hexagons.

In Fig. 4b the foil is imaged at the [233] pole with two reflections $[0\bar{2}2]$ and $[\bar{3}\bar{1}3]$ such that all four variants are seen. Imaging with only $[0\bar{2}2]$, e.g., g = AB, would put the γ loops out of contrast as $g \cdot b_\gamma = 0$. The γ plane is at a shallower inclination than α or β and this is confirmed by the appearance of the γ loop in the image. Loops α and β, by virtue of their high inclinations appear narrow. Hexagonal loops in the foil plane, δ, appear by m-term contrast [7a] symmetric with respect to g.

That the habit planes of these defects are (111) is concluded from trace analysis. Their sides are accurately along $\langle 110 \rangle$ and only the (111) planes contain three $\langle 110 \rangle$ directions. Further, if the loops are regular hexagons the ratio of the length of the sides gives the cosiness of the angles of inclination. This method gave angles of 63° and 68° for the inclined loops β and α respectively. This is in reasonable agreement with the fact that the inclined (111) planes make 70° angles with the (111) plane of the foil. Lastly, the loops show displacement fringe contrast implying that they are faulted and, therefore, must lie on $\{111\}$ planes. The displacement vectors for the large majority of the loops are not lattice translations i.e., not $\frac{a}{2}\langle 110 \rangle$, as suggested by earlier results [1-3] but rather $\frac{a}{x}$ [111]. Certain contrast effects suggest that x is not exactly three. Segregation of dopants or impurities on the stacking fault probably changes the displacement vector slightly. A result which is consistent with this hypothesis may be seen at the

unfaulted loop at A (Fig. 4b) which appears dark inside. This contrast effect may be explained if it is assumed that the segregation remains inside the loop even after it has transformed to a "perfect" loop. There would still be a small displacement remaining in the [111] direction which could give rise to this dark center.

6. Determination of Loop Type

The analysis confirming that the loops on the inclined planes are interstitial is given in Fig. 5. Figure 5a shows the situation as found in the micrograph in Fig. 2. In terms of the FSRH [7] convention only extrinsic defects on the inclined planes are expected to give images consistant with those observed experimentally in Fig. 2a (Fig. 5b). A separate analysis showing the rotations of the planes around the defects is also given in Fig. 5b. Here use is made of the fact that at the s>o condition a clockwise rotation of the crystal planes brings them into the reflecting condition. This analysis also confirms the interstitial nature of the defects on the inclined planes. Only the sense of the inclination of the habit plane and the displacement vector are involved in this analysis.

Similar analysis of the loops in the plane of the foil shows that they are also interstitial type. The resulting distribution of defects is shown in Fig. 5c.

7. Conclusions

The loops are shown to be interstitial type. The habit planes of the loops have been determined to be the four {111} planes and the displacements are of the type $\frac{a}{x}\langle 111\rangle$ with x not being exactly three, probably because of the segreation of dopants or impurities on the stacking fault. There are a few perfect loops which also show evidence of precipitation or segregation remaining inside the loop. The distribution of defects in Fig. 5c suggests that the loops are formed by the clustering of interstitials on close packed planes, which subsequently grow during the annealing treatment.

It has been mentioned that varying accounts exist regarding the nature of defects in P^+ ion-implanted silicon. Studies in progress indicate that defect morphology and type is very sensitive to the presence of impurity (e.g., oxygen), the element used for dopant of substrate prior to implantation and type of substrate (n or p type). Therefore, the different results of other workers may be caused by differences in the material or implantation procedure.

Acknowledgements

We thank Dr. V. G. K. Reddi of Fairchild R&D Division for supply of samples. The inspiration for this paper is entirely W. L. Bell's. This work has been done under the auspices of the U. S. Atomic Energy Commission.

References

[1] M. Tamura, T. Ikeda and N. Yoshihiro, J. of the Japan Soc. of Appl. Phys. 40, 9 (1971).

[2] W. K. Wu and J. Washburn, J. Appl. Phys. 45(3), 1085 (1974).

[3] S. M. Davidson and G. R. Booker, Rad. Effects 6, 33 (1970).

[4] R. W. Bicknell, Ph. D. Thesis, University of London, 1971 and private communication.

[5] M. L. Jenkins, D. J. H. Cockayne and M. J. Whelan, J. Microscopy 98, 155 (1973).

[6] D. J. H. Cockayne, I. L. F. Ray and M. J. Whelan, Phil. Mag. 20, 1265 (1969).

[6a] K. Seshan, Proc. 32nd Annual EMSA Meeting, St. Louis (1974).

[7] P. B. Hirsh, et al., Electron Microscopy of Thin Crystals (Butterworths, London, 1965), p. 265.

[7a] Ibid, p. 261.

[8] W. L. Bell and G. Thomas, Phys. Stat. Sol. 12, 843 (1965).

Figure Captions

Fig. 1. (a) Shows the crystal with the $[\bar{1}\bar{1}\bar{1}]$ tetrahedron as seen in an emulsion side down print. (b) Shows that the 180° ambiguity is resolved by noting the position of the $[2\bar{1}1]$ pole in the Kikuchi pattern. The correctly oriented tetrahedron (including 180° inversion and magnetic lense rotation) projected above the crystal is shown, as is the crystal with the β and γ planes inclined in the proper sense. All pictures used for the analysis were images at $s>o$, with the reflection inside the Ewald sphere as shown.

(c) The [111] stereogram from which the correct crystallographic directions may be obtained. E.g., the operation reflection in Fig. 2a is along $\overline{BC}$ or $[02\bar{2}]$.

Fig. 2. Shows the stereo-pair obtained while tilting the crystal to determine the position of the $[\bar{2}\bar{1}\bar{1}]$ pole. Tetrahedra are drawn below to coincide with the defect directions. E.g., rod AC lies along the side marked AC. Notice the change in the position of the rod DB on tilting from the $[\bar{1}\bar{1}\bar{1}]$ to the $[\bar{2}\bar{1}\bar{1}]$ pole. Viewing these images through a stereo viewer shows that B is far below D; i.e., B is near the top of the foil. Loops marked γ show inside contrast; β shows outside contrast. These are assumed inclined in the sense of the planes ADB and ADC. This assumption is validated by weak-beam images (Fig. 4).

Fig. 3. Shows how dark field images may be used to determine the correct orientation of the crystal. Figure 3a ($s<o$) the top of the foil is in good contrast and the top end of the inclined rod at B is seen. In Fig. 3b ($s>o$) the bottom of the rod D is seen in good oscillating contrast. The crystal must then be oriented as shown in the line drawings and this procedure easily eliminated the 180° ambiguity.

Fig. 4. Shows weak-beam images at the [211] and [233] poles. These images show that the loops are hexagonal and the distributed on the four {111} planes. Figure 4a shows the loops at the [211] pole. Defect marked B lies edge one. α and γ appear steeply inclined to the foil. δ on the plane of the foil ABC

appears hexagonal. In Fig. 4b the foil is imaged at the [233] pole. The plane ADC is at a shallower angle than α or β and this is seen in the image. A three beam condition with the reflections $[0\bar{2}2]$ and $[\bar{3}\bar{1}3]$ operating was used for this image. At the unfaulted loop at A has a strong black contrast inside the loop suggesting precipitation inside the loop.

Fig. 5. (a) Summarizes the experimental situation in Fig. 2a. The crystal with the relevant planes is shown with the observed nature of the images. At this stage only the sense of inclination of the defects need be known. (b) Shows the formal FSRH (perfect crystal) analysis [7]. For outside images (s>o) $g \cdot R$ is negative and for inside images $g \cdot R$ is positive. Therefore, the displacement vectors must be as shown in order to agree with the observation of Fig. 2a. The analysis is also done in terms of the rotations of the planes. At s>o a clockwise rotation of the planes brings the crystal into the reflecting position. The rotations around interstitial loops give the required images. It is concluded that the loops on the inclined planes are interstitial. (c) Shows the distribution of defects in the crystal. The distribution suggests a ripening of interstitial clusters during the annealing treatment.

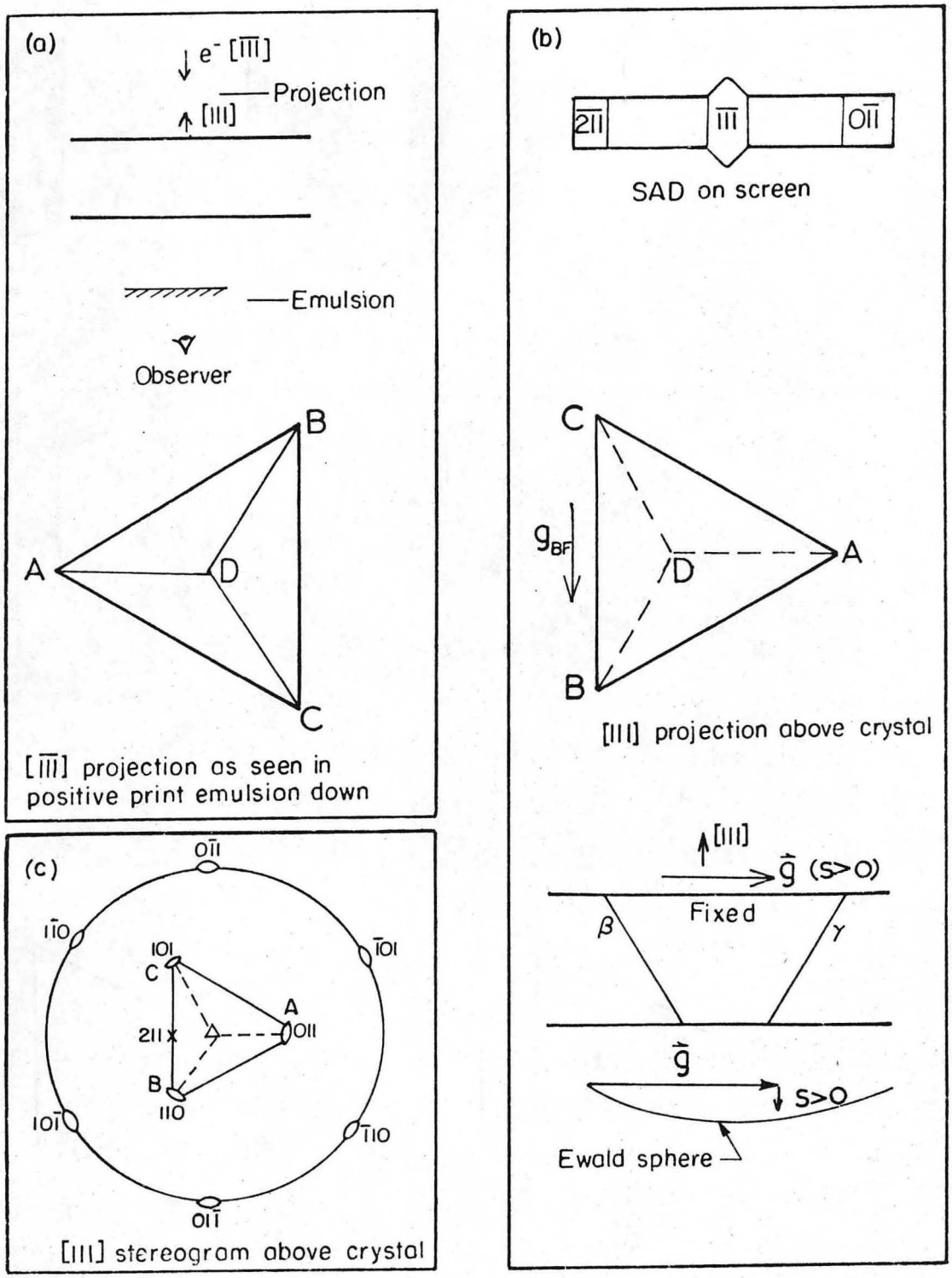

XBL745-6242

Fig. 1

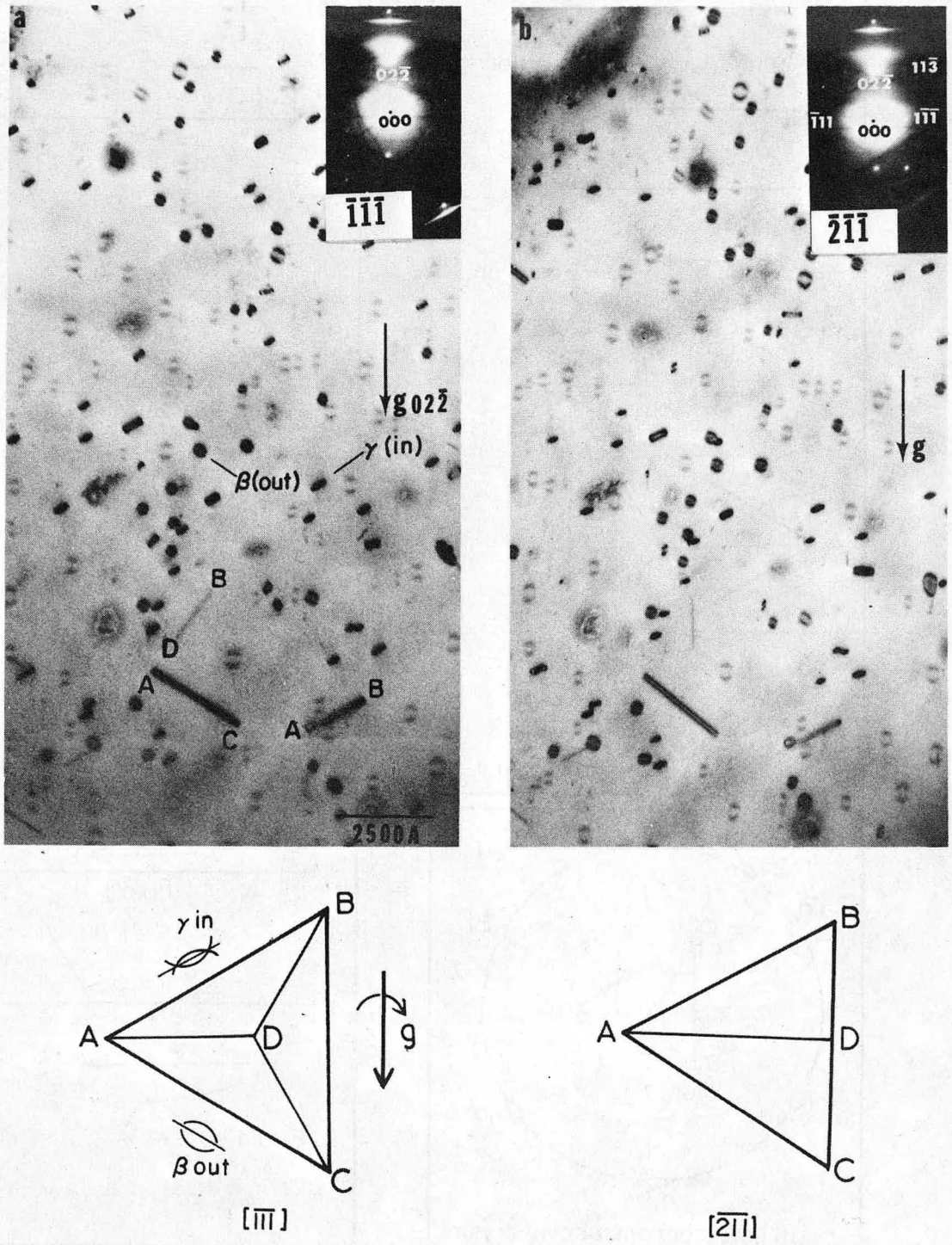

XBB 745-3334

Fig. 2

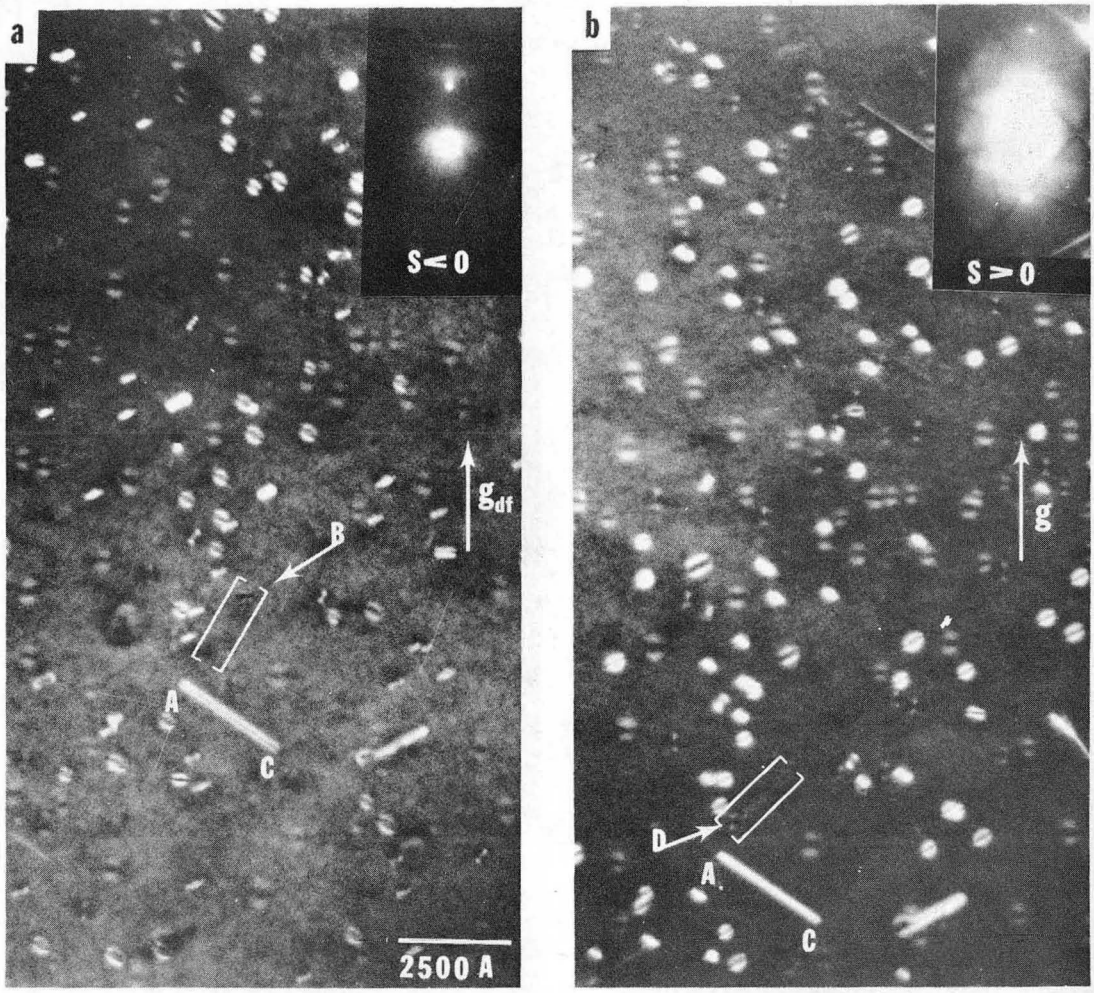

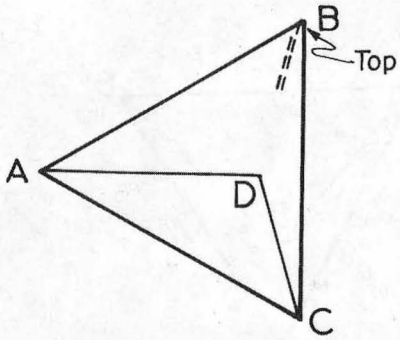

S<O Top of foil in good contrast

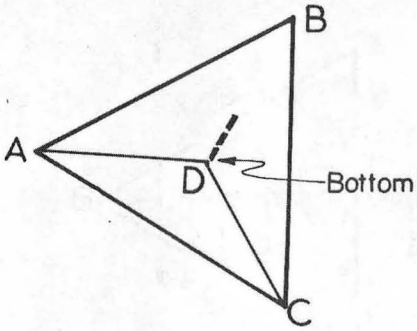

S>O Bottom of foil in good contrast

XBB 745-3333

Fig. 3

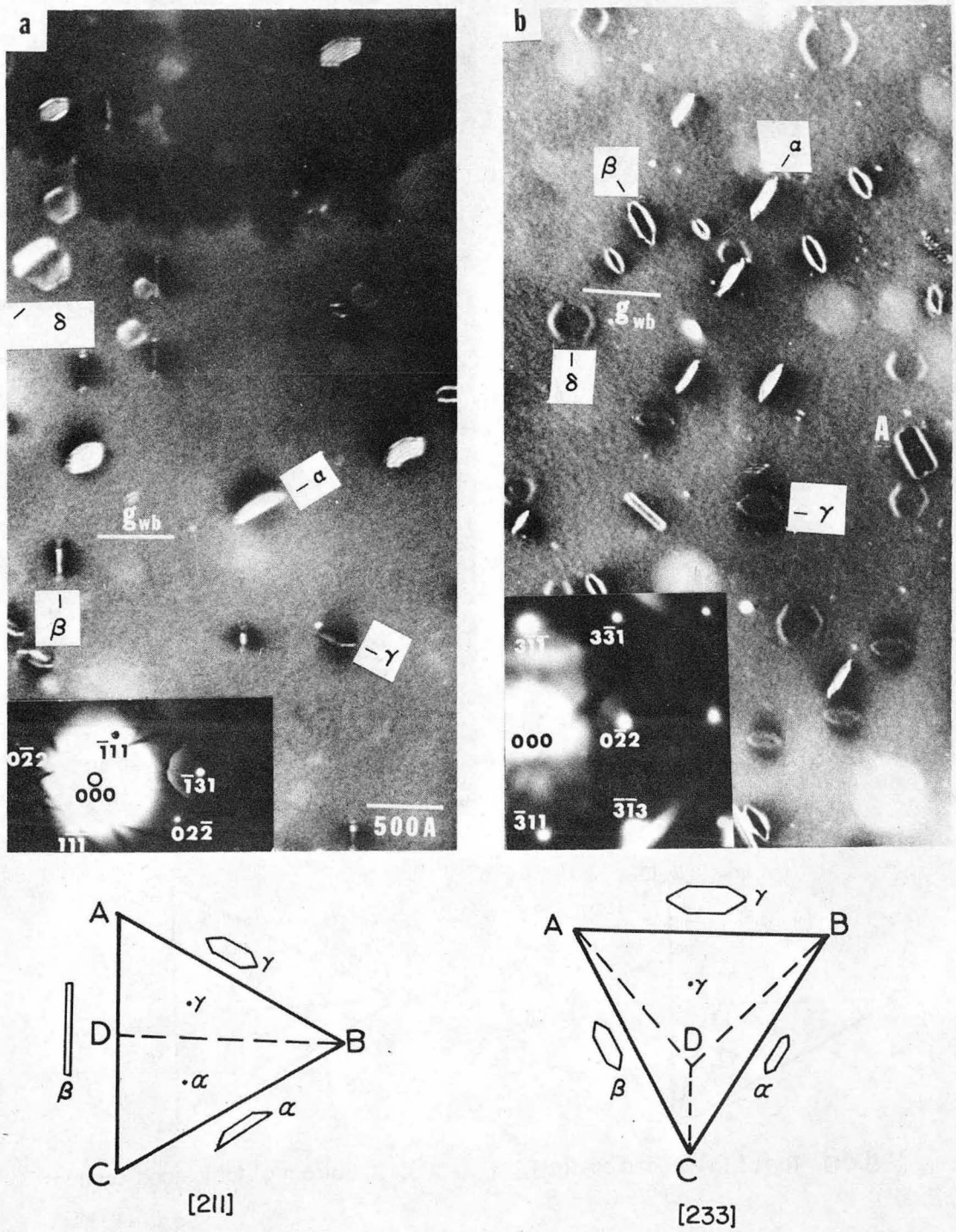

XBB 745-3335

Fig. 4

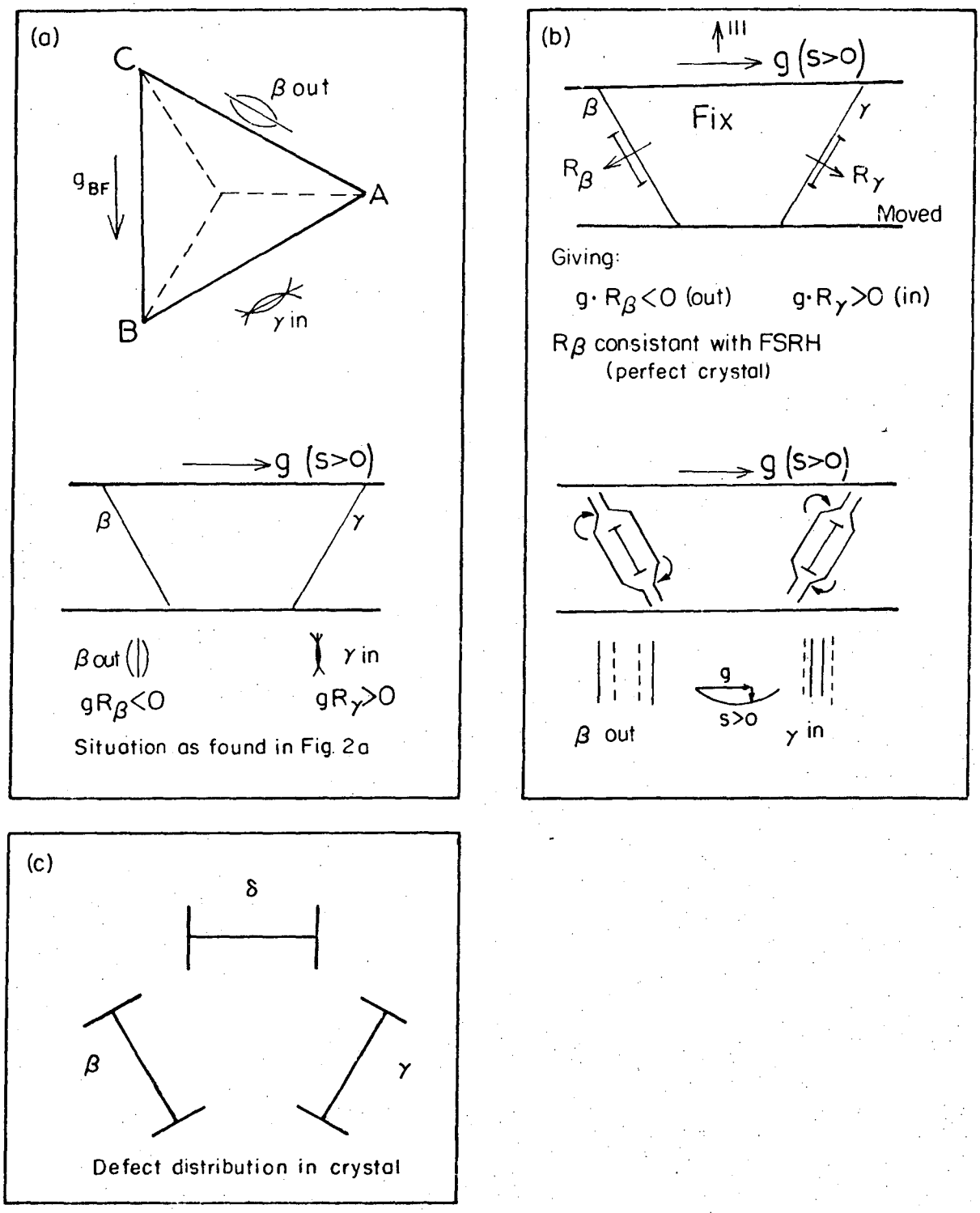

XBL 745-6241

Fig. 5

LEGAL NOTICE

This report was prepared as an account of work sponsored by the United States Government. Neither the United States nor the United States Atomic Energy Commission, nor any of their employees, nor any of their contractors, subcontractors, or their employees, makes any warranty, express or implied, or assumes any legal liability or responsibility for the accuracy, completeness or usefulness of any information, apparatus, product or process disclosed, or represents that its use would not infringe privately owned rights.

TECHNICAL INFORMATION DIVISION
LAWRENCE BERKELEY LABORATORY
UNIVERSITY OF CALIFORNIA
BERKELEY, CALIFORNIA 94720